Tran. Natl. Acad. Sci. Azerb. Ser. Phys.-Tech. Math. Sci.
Mechanics, **46** (7), 38–49 (2026);
https://doi.org/10.30546/2706-7734.46.7.2026.045

Modeling an arc-shaped adhesive crack in a unidirectional fiber-reinforced composite under longitudinal shear

Rafail K. Mekhtiev

Received: 25.08.2026 / Revised: 10.02.2026 / Accepted: 12.05.2026

Abstract. *This paper investigates, by combining theoretical and numerical approaches, the mechanical behavior of an arcuate adhesion (debond) crack located at the fiber–matrix interface in a unidirectional fiber-reinforced polymer-matrix composite subjected to longitudinal sliding (Mode III, antiplane) loading. The composite medium is modeled as a transversely isotropic elastic material. The distribution of interfacial shear stresses, stress concentration at the crack tip, and the energy release rate required for crack propagation are evaluated within the framework of a cohesive zone model (CZM). The crack growth threshold is determined using the energy criterion $G \geq G_c$, where G is the interfacial energy release rate and G_c is the critical fracture energy inherent to the material–interface system. Example calculations and parametric studies show that the stress field localizes at the crack tip and the energy dissipation intensifies; increasing the interface stiffness k_i suppresses crack advance and limits energy spreading. The proposed modeling scheme provides a practical methodological basis for assessing microcracks in composite structures, selecting interface-strengthening strategies, and improving structural durability in high-reliability aerospace and automotive applications.*

Keywords. adhesion cracks · fibrous composite · longitudinal sliding (Mode III) · interface stiffness · cohesive zone model · energy dissipation · fracture mechanics · transversely isotropic medium · FEM · structural stability

Mathematics Subject Classification (2010): 74A40, 74S15

1 Introduction

The widespread use of composite materials in aerospace, automotive, energy, and mechanical structures is driven by their high specific strength, low weight, and design flexibility [3, 9]. In particular, in unidirectional fiber-reinforced polymer-matrix composites, the major

R.K. Mekhtiev
Azerbaijan State University of Petroleum and Industry, 20 Azadlig Avenue, Baku, Azerbaijan
E-mail: rafail60mehtiev@mail.ru

portion of load-carrying capacity is provided by the fibers, while the matrix binds the fibers, transfers the load, and maintains geometric stability [9].

A significant part of the failure mechanisms in these materials occurs at the fiber–matrix interface. Since stress transfer from fibers to matrix under external loading depends directly on interface quality, interfacial weakening (adhesion loss, delamination, micro-bond rupture) can lead to the formation of arcuate or partial debond cracks [12, 14]. Under longitudinal sliding (Mode III) loading, interfacial shear stresses dominate; therefore, sharp stress concentration and energy accumulation develop near the crack tip, accelerating crack propagation [6, 19].

Classical linear elastic fracture mechanics (LEFM) often predicts singular (infinite) stresses at the crack tip and thus cannot fully capture physically observed gradual softening and progressive bond breaking in real materials [16]. For this reason, cohesive zone models have been widely adopted over recent decades because they provide a more physically realistic description of finite crack-tip stresses and energy-based fracture mechanisms [19].

The aim of this study is to model the stress and energy distributions for an arcuate adhesion crack at the fiber–matrix interface in a unidirectional composite under longitudinal sliding loading, and to systematically evaluate how key parameters (interface stiffness, fiber volume fraction, and elastic property ratios) influence crack development.

2 Literature review

Fundamental references on failure mechanisms in fiber composites indicate that fracture typically develops through a combination of fiber breakage, matrix cracking, and interfacial debonding processes [9]. Although classical elasticity and LEFM-based models are useful for simplified descriptions, their accuracy is limited in real systems due to heterogeneous microstructure, anisotropic mechanical response, and nonlinear separation along the interface [3, 18].

Within the framework of transversely isotropic and laminate composite mechanics, differences in mechanical properties along the fiber direction and in the transverse direction affect both the stress field and the crack growth direction [3, 18]. Because shear components are dominant in antiplane (Mode III) conditions, analysis of interface cracks under longitudinal sliding occupies a special place [6, 16].

Cohesive zone models account for the “process zone” (softening zone) near the crack tip and link failure to energy via traction–separation laws, allowing crack initiation and propagation to be assessed in a unified framework [19]. This approach more adequately describes progressive bond rupture, micro-friction associated with sliding, and energy absorption at the fiber–matrix interface [12, 19].

Overall, the literature shows that the stability of interface cracks in fiber composites is governed not only by the maximum stress, but also by the energy release rate, interface stiffness, and the ratios of material properties [6, 12]. Therefore, multifactor models combining analytical and FEM-based methods are more appropriate for engineering applications.

3 Research aim and objectives

Studies in fracture mechanics of fiber-reinforced composites indicate that the overall durability of a material depends not only on the properties of the fibers and matrix, but also on processes occurring in their boundary region—the interface. In particular, under longitudinal sliding loading, the formation and growth of arcuate adhesion cracks at the fiber–matrix interface can severely weaken the structural integrity of the composite.

3.1 Main aim

To model the mechanical behavior of an arcuate adhesion crack at the fiber–matrix interface in a composite under longitudinal sliding, and to investigate the crack-tip stress and energy distributions from both theoretical and applied perspectives. For this purpose, the main mechanical parameters influencing the crack growth trajectory are identified, and the localization of the stress field and the intensity of energy dissipation are evaluated.

3.2 Main objectives

- **Review of the scientific literature:** systematic study of previous research on fracture mechanics of fiber composites, cohesive zone models, and analysis of interfacial stresses;
- **Model formulation:** mathematical modeling of an arcuate crack at the fiber–matrix boundary in a transversely isotropic elastic composite under longitudinal sliding;
- **Boundary and equilibrium conditions:** formulation of appropriate boundary conditions and static equilibrium equations for accurate stress and displacement evaluation;
- **Application of the cohesive zone model:** definition of energy-based boundary functions and fracture criteria along the cohesive zone near the crack tip;
- **Energy dissipation calculation:** analysis of the energy dissipation level along and around the crack and assessment of the stability criterion;
- **Parametric investigation:** study of the effects of fiber volume fraction, interface stiffness, and elastic modulus ratios on crack growth and stress distribution;
- **Engineering applicability:** evaluation of the potential of modeling results for practical engineering structures, especially in aerospace and automotive industries.

4 Mathematical model and methodology

4.1 Transversely isotropic representation of the medium

Because elastic properties differ along the fiber direction and in the transverse direction in unidirectional fiber-reinforced composites, the medium is modeled as transversely isotropic elastic [3, 18]. The main elastic parameters include:

- E_1—elastic modulus along the fiber direction;
- $E_2 = E_3$—elastic moduli in the transverse directions;
- $G_{12} = G_{13}$—shear moduli in fiber–transverse planes;
- $\nu_{12} = \nu_{13}$ and ν_{23}—Poisson's ratios.

Based on these parameters, linear elastic relations are established and the stress–strain relation accounts for anisotropic mechanical response [3, 18].

4.2 Longitudinal slip (Mode III, antiplane) scheme

The displacement in the longitudinal slip mode is mainly described by the $u_z(x, y)$ component and the main shear stresses are [7, 10]:

$$\tau_{xz} = G_{13}\frac{\partial u_z}{\partial x}, \qquad \tau_{yz} = G_{23}\frac{\partial u_z}{\partial y}. \tag{4.1}$$

The equilibrium equation (without considering body forces) is written as follows:

$$\frac{\partial \tau_{xz}}{\partial x} + \frac{\partial \tau_{yz}}{\partial y} = 0. \tag{4.2}$$

Substituting expression (4.1) into (4.2), the following governing equation is obtained:

$$\frac{\partial}{\partial x}\left(G_{13}\frac{\partial u_z}{\partial x}\right)+\frac{\partial}{\partial y}\left(G_{23}\frac{\partial u_z}{\partial y}\right)=0. \tag{4.3}$$

This approach is consistent with the standard antiplane formulation of Mode III crack mechanics [6, 16].

4.3 Interfacial stress distribution and stress concentration

For a simplified analytical estimate, the interfacial shear stress is assumed to decrease linearly away from the crack tip:

$$\tau(x)=\tau_{\max}\left(1-\frac{x}{l}\right), \qquad 0\le x\le l, \tag{4.4}$$

where x is the coordinate along the interface from the crack tip, l is the characteristic crack (or cohesive zone) length, and $\tau_{\max}$ is the maximum interfacial shear stress at the crack tip.

Nominal (average) breaking stress:

$$\bar{\tau}=\frac{1}{l}\int_0^l \tau(x)\,dx. \tag{4.5}$$

When expression (4.4) is substituted into (4.5),

$$\bar{\tau}=\frac{\tau_{\max}}{2}. \tag{4.6}$$

For nominal stress $\tau_{\text{nom}}=\bar{\tau}$, the stress concentration factor is

$$K_t=\frac{\tau_{\max}}{\bar{\tau}}. \tag{4.7}$$

Considering expression (4.6) in (4.7),

$$K_t=2. \tag{4.8}$$

This parameter provides a compact characterization of the influence of interface weakness on failure [6, 16].

4.4 Cohesive zone model (CZM) and energy criterion

Progressive bond degradation at the crack tip is described using CZM. A linear softening traction–separation law is adopted:

$$\tau(\delta)=\tau_{\max}\left(1-\frac{\delta}{\delta_c}\right), \qquad 0\le\delta\le\delta_c, \tag{4.9}$$

where δ is the sliding displacement and δ_c is the critical displacement.

The energy dissipation rate (interface dissipation energy) is

$$G=\int_0^{\delta_c}\tau(\delta)\,d\delta. \tag{4.10}$$

Integrating expression (4.9) in (4.10) gives

$$G = \int_0^{\delta_c} \tau_{\max} \left(1 - \frac{\delta}{\delta_c}\right) d\delta = \frac{\tau_{\max}\delta_c}{2}. \tag{4.11}$$

The crack propagation condition is given by the energy criterion

$$G \geq G_c, \tag{4.12}$$

where G_c is the critical fracture energy of the interface [19]. Thus, from expressions (4.11) and (4.12), the crack progression condition is written directly as

$$\frac{\tau_{\max}\delta_c}{2} \geq G_c. \tag{4.13}$$

In this work, energy is expressed in $\mathrm{N/mm}$. Since

$$1\ \mathrm{MPa} \cdot \mathrm{mm} = 1\ \frac{\mathrm{N}}{\mathrm{mm}^2} \cdot \mathrm{mm} = 1\ \mathrm{N/mm}, \tag{4.14}$$

the units used in the numerical example are mutually consistent.

4.5 Numerical modeling using FEM

In addition to analytical estimates, a 2D FEM model is employed to more realistically capture stress localization and boundary effects [18]. In the model:

- the bottom boundary is fixed (clamped);
- a longitudinal sliding load is applied on the top boundary;
- the interface crack and cohesive zone parameters are introduced along the interface.

This approach enables visualization and numerical quantification of crack-tip stress accumulation and energy distribution.

The studied composite consists of a polymer matrix reinforced with unidirectional fibers. Fibers mainly provide load transfer, and the matrix bonds them together. The interface region is mechanically weaker and can serve as a crack initiation site. A schematic cross-section of the composite is shown in Fig. 4.5.

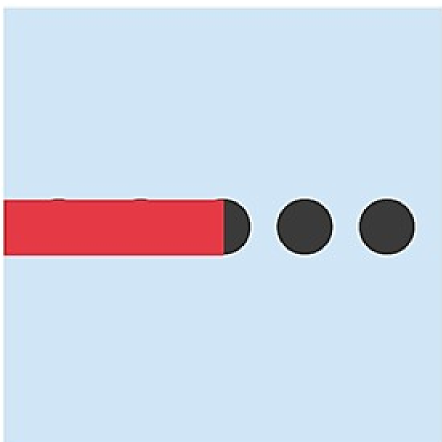

Fig.4.1. Cross-section of the composite structure.

The mutual positioning of fibers, matrix, and the interface region in the microstructure is presented in Fig. 4.5. This visualization clearly reflects functional regions of the internal structure and their mechanical roles. The light blue region represents the matrix phase, which forms the structure, transfers load between fibers, holds fibers in place, and helps distribute external loads. The dark circles represent the fibers, aligned primarily in the longitudinal direction, carrying the majority of the load and exhibiting high stiffness and strength. The bright red band represents the adhesion crack along the fiber–matrix interface, which symbolizes microcracks where stresses concentrate and failure may initiate.

In this study, a longitudinal sliding load is applied to the arcuate adhesion crack. The load acts mainly along the fiber axis and generates interfacial shear stresses. The stress distribution reaches a maximum near the crack tip and drives crack growth. This mechanical action is schematically illustrated in Fig. 4.5.

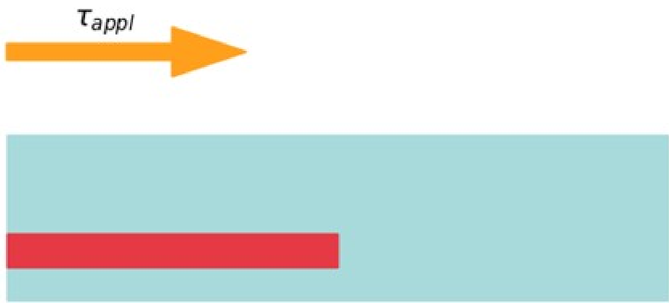

Fig.4.2.Shear loading scheme: an interface crack under longitudinal sliding (Mode III) loading and the applied shear stress.

5 Example calculations and results

5.1 Material and model parameters

To more realistically evaluate the growth of adhesion cracks at the fiber–matrix interface, example calculations and parametric analyses are carried out. The parameters are chosen for a carbon fiber–epoxy system and used as input for the transversely isotropic elastic model and the cohesive zone model [19].

Table 1 Mechanical and cohesive parameters used in the modeling of a unidirectional fiber-reinforced composite.

Parameter	Symbol	Value	Unit
Fiber elastic modulus	E_f	210	GPa
Matrix elastic modulus	E_m	3.5	GPa
Fiber volume fraction	V_f	0.55	–
Poisson’s ratio (fiber–matrix)	ν_{12}	0.28	–
Interface stiffness	k_i	2.0×10^3	MPa/mm
Crack length	l	2.0	mm
Maximum cohesive shear stress	$\tau_{\max}$	50	MPa
Critical displacement	δ_c	0.015	mm

The material and cohesive parameters used in the model are given in Table 1. These values fall within typical engineering ranges for carbon-fiber-reinforced epoxy composites and are used as input in analytical calculations and FEM simulations.

5.2 Analytical evaluation of interfacial shear stress along the crack

According to the adopted distribution,

$$\tau(x) = \tau_{\max}\left(1 - \frac{x}{l}\right).$$

For example,

$$x = 0:\ \tau(0) = \tau_{\max} = 50\ \mathrm{MPa}, \qquad x = l = 2.0\ \mathrm{mm}:\ \tau(l) = 0\ \mathrm{MPa}.$$

The average shear stress is

$$\bar{\tau} = \frac{1}{l}\int_0^l \tau(x)\,dx = \frac{\tau_{\max}}{2} = 25\ \mathrm{MPa}.$$

Thus, the stress concentration factor becomes

$$K_t = \frac{\tau_{\max}}{\bar{\tau}} = \frac{50}{25} = 2.$$

This result indicates that the crack-tip shear stress is twice the nominal level and confirms that failure risk increases primarily in the crack-tip region [6,16].

5.3 Energy release rate calculation (CZM)

The energy release rate is

$$G = \int_0^{\delta_c} \tau(\delta)\,d\delta = \frac{\tau_{\max}\delta_c}{2}.$$

Substituting numerical values gives

$$G = \frac{50 \times 0.015}{2} = 0.375\ \mathrm{N/mm}.$$

Therefore, if the critical interface energy satisfies $G_c < 0.375\ \mathrm{N/mm}$, crack propagation is energetically feasible and the fracture process initiates [19].

To evaluate local energy dissipation and stress concentration at the crack tip, the cohesive zone model is applied. The typical traction–separation relation for the cohesive zone is shown in Fig. 5.3.

Figure 5.3 presents a typical shear traction–displacement τ–δ relation in the cohesive zone near the crack tip. The blue curve shows how traction decreases linearly with increasing displacement until it reaches zero. The shaded area represents the dissipated energy $G = \int_0^{\delta_c} \tau(\delta)\,d\delta$, which is a key parameter defining the crack growth threshold. This plot is essential for energy-based fracture assessments, since it accounts not only for maximum stress but also for energy dissipation and damage tendency.

Figure 5.3 shows the interfacial shear stress distribution $\tau(x)$. As seen from the graph, the shear stress reaches the maximum $\tau_{\max}$ at the crack tip and decreases with distance along the crack, approaching zero at $x = l$. This confirms that stress concentration forms at the crack tip and that the critical zone governing failure is located at the crack tip. This type of distribution is a typical analytical approximation for assessing interface crack growth under Mode III loading.

The fact that interfacial shear stress is maximal at the crack tip and decreases with distance, as observed in Fig. 5.3, confirms stress concentration in the crack-tip region. Such

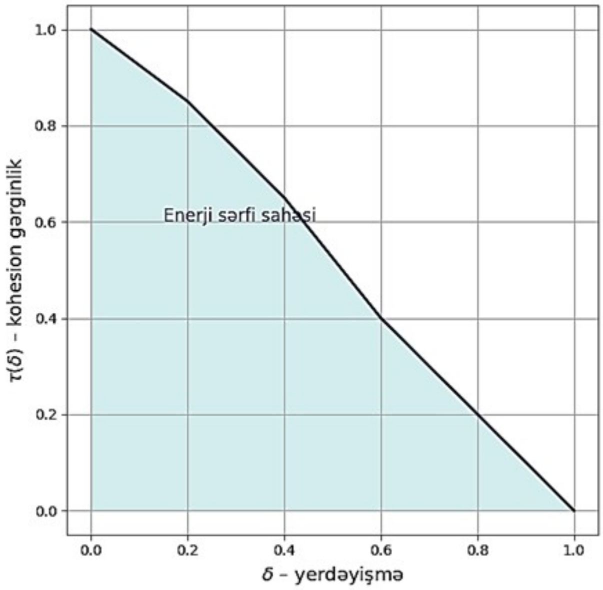

Fig.5.1. Cohesive zone model curve.

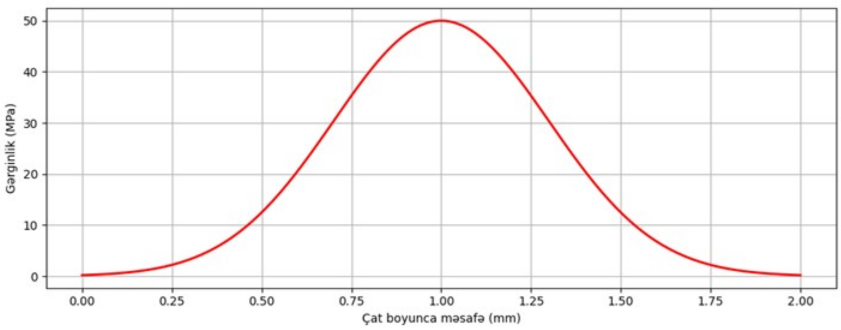

Fig.5.2.Shear stress distribution along the crack.

analyses also provide a basis for verifying cohesive zone models and for practical validation of mathematical modeling results.

The dependence of dissipated energy on interface stiffness is important from an engineering standpoint. A stiffer interface provides higher resistance and therefore dissipates less energy. Figure 5.3 shows the general trend between energy release rate G and interface stiffness k_i. As k_i increases, sliding displacements at the interface are constrained, the deformation zone "narrows," and energy absorption decreases. In other words, a stiffer interface stabilizes load transfer, weakening the effective energy distribution required for crack advance. This result explains the beneficial effect of interface strengthening measures (surface treatment, coatings, appropriate coupling systems) on crack durability.

As interface stiffness increases, plastic deformation in the interface region decreases, meaning less internal friction and more effective load transfer. Consequently, energy loss during transfer is reduced and total energy dissipation decreases. This behavior is noticeable in the range of interface stiffness from 1.0 MPa/mm to 3.0 MPa/mm. In addition, increased stiffness helps preserve structural integrity and suppress microcrack initiation. A stiffer interface distributes stresses more uniformly and prevents local energy accumulation.

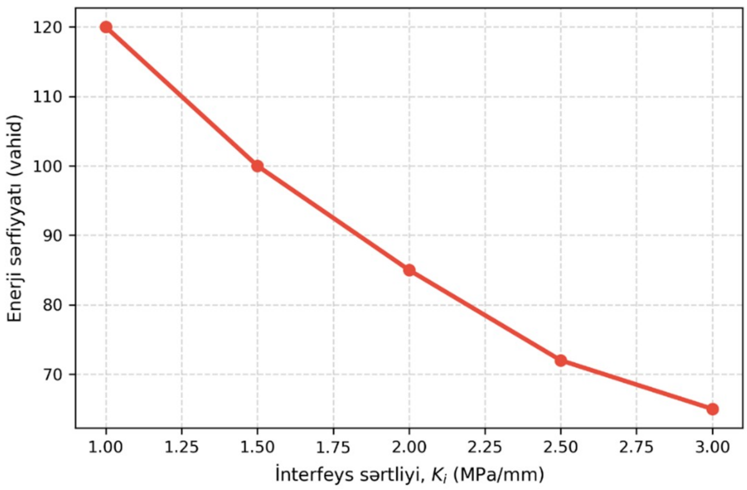

Fig.5.3. Energy release rate G versus interface stiffness k_i (inverse trend).

Thus, Fig. 5.3 indicates that increasing interface stiffness plays an important role in composite optimization and can be considered a key technological parameter for improving energy efficiency and crack resistance.

To analyze crack growth in composite structures, simulations based on the proposed cohesive zone model are carried out. Using FEM, the crack-tip stress distribution and interfacial energy distribution are determined. Model inputs are based on realistic material properties.

Figure 5.3 shows the simulation environment developed using FEM and boundary conditions. Layers and inclusions representing microstructural features are shown. Different mesh densities are used in upper and lower regions to model different material characteristics.

The bottom boundary is fixed, and mechanical loading is applied from the top. The longitudinal direction (X-axis) is indicated and deformation/energy transfer is tracked along it. Circular inclusions represent the stiff phase in the composite. The parameters provided correspond to the main mechanical and physical inputs: the modulus ratio of reinforcement to matrix, the critical energy release rate, the stiffness parameter, and the fiber volume fraction.

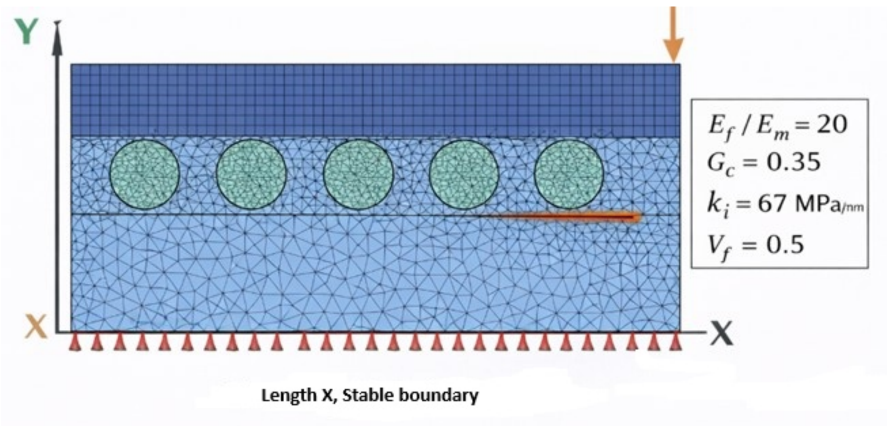

Fig.5.4. Simulation environment (FEM model with boundary conditions).

Accordingly, the FEM modeling environment and boundary conditions shown in Fig. 5.3 form the computational scheme for numerical analysis.

Figure 5.3 shows the stress field obtained from the FEM simulation. The stress component distribution within the model is presented in MPa. The color scale indicates stress intensity. Red/orange regions correspond to the maximum stresses (approximately 80–90 MPa), while blue regions correspond to minimal stresses (0–10 MPa).

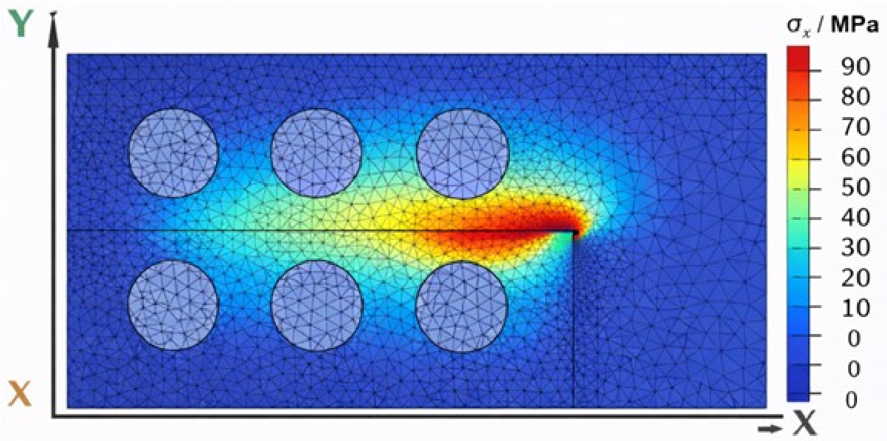

Fig.5.5.FEM result: stress field distribution.

The circular inclusions again represent the reinforcing phase. Higher stress concentration is observed near the crack tip on the right side, demonstrating how stresses accumulate in critical regions under loading. Such simulations are valuable for identifying weak points and potential fracture initiation zones. The stress increase aligned with the crack direction supports damage prediction in structural mechanics. Thus, the analysis provides essential information for improving durability and proposing optimal design solutions. Consequently, stress localization near the crack tip observed in Fig. 5.3 is qualitatively consistent with the analytical predictions.

6 Discussion

The results show that the behavior of an interface crack under longitudinal sliding is governed by the combined effects of two mechanisms: stress localization at the crack tip and energy absorption in the cohesive zone. The analytical distribution shown in Fig. 5.3 confirms the maximum crack-tip shear stress and the decrease of $\tau(x)$ along the crack, indicating that the crack-tip region is the governing zone controlling crack advance.

From an energy viewpoint, the relation $G = \tau_{\max}\delta_c/2$ directly links crack propagation capability to cohesive parameters. In the example, $G = 0.375\ \mathrm{N/mm}$; therefore, if G_c is lower than this value, crack propagation is energetically favorable. This provides a more stable and physically meaningful assessment than a "maximum stress only" criterion.

Parametric trends show that increasing interface stiffness k_i suppresses crack propagation (Fig. 5.3). This is a crucial design signal: interface strengthening methods (fiber surface treatment, coupling agents, coating layers) can enhance crack durability and improve service reliability. Although increasing fiber volume fraction V_f raises load-carrying capacity, if the interface is weak the crack-tip stresses can become more critical; hence, increasing fiber content for high strength must be balanced by interface quality.

FEM results shown in Figs. 5.3 and 5.3 qualitatively agree with analytical predictions: maximum stresses concentrate near the crack tip, and the high stress gradient indicates that crack growth will initiate from that region.

Overall, the results demonstrate the effectiveness of energy-based approaches and cohesive zone models for modeling crack growth at the fiber–matrix interface. The study confirms that applying a multifactor approach (stress, stiffness, energy, fiber volume fraction, etc.) provides a more accurate prediction of real mechanical behavior than elasticity theory alone. The findings have application potential in high-reliability fields such as aerospace and automotive industries.

7 Conclusion

This study modeled the behavior of an arcuate adhesion crack at the fiber–matrix interface in a unidirectional fiber-reinforced composite under longitudinal sliding (Mode III) by combining an analytical approach (simplified stress distribution plus cohesive zone model) and FEM. The main conclusions are as follows.

1 **Stress concentration and crack-tip effect.** Analytical and FEM results show that the maximum interfacial shear stress occurs at the crack tip and decreases with distance (Figs. 5.3 and 5.3). This confirms that crack initiation and growth are governed by the crack-tip region and that interface weakness directly affects structural durability.

2 **Validation of the energy-based stability criterion.** In the cohesive zone model, the energy release rate is

$$G = \frac{\tau_{\max}\delta_c}{2}.$$

In the example, $G = 0.375\ \mathrm{N/mm}$, showing that crack growth depends directly on the critical energy parameter G_c.

3 **Effect of interface stiffness on crack durability.** Parametric analysis indicates that increasing k_i reduces deformation amplitude in the cohesive zone and limits energy dissipation (Fig. 5.3), slowing crack propagation and improving overall mechanical stability.

4 **Effect of elastic modulus ratio.** As the modulus ratio increases, load transfer shifts more strongly to the fibers and the interfacial stress distribution changes, indicating that interface quality is critical for high-stiffness composites.

5 **Consistency between FEM and analytical predictions.** FEM qualitatively confirms analytical predictions, especially stress localization near the crack tip and the correspondence with the energy dissipation zone, supporting the physical adequacy of the cohesive zone model.

Thus, the modeling demonstrates that interface stiffness and cohesive parameters are the key factors controlling crack growth in unidirectional fiber composites, and optimizing these parameters is an effective engineering strategy to improve mechanical reliability.

Recommendations and application prospects

1 **Material selection for interface strengthening:** selecting interface systems with higher adhesion capability and chemical/mechanical compatibility is recommended.

2 **Structural optimization controlling crack orientation:** optimizing fiber arrangement, particularly increasing fiber density in critical zones, can help suppress crack growth.

3 **Multiscale simulation:** extending the present 2D approach to 3D analyses will improve accuracy for real structures.

4 **Experimental validation:** experiments should be conducted on analogous physical models to calibrate and validate the numerical model.
5 **Engineering applications:** the approach is applicable in aerospace, automotive, construction, and energy sectors for assessing safety in heavily loaded composite components.
6 **Integration into digital twin systems:** integrating the simulation scheme into Digital Twin platforms can enable real-time monitoring and prediction of crack evolution for structural health management.

References

1. Barbero, E. J. (2010). *Introduction to composite materials design* (2nd ed.). CRC Press. https://doi.org/10.1201/9781439894132
2. Belyaev, N. M., & Kulakov, V. L. (2003). *Osnovy rascheta konstruktsiy iz kompozitsionnykh materialov* [Fundamentals of structural analysis of composite materials]. Mashinostroenie.
3. Çelik, R. (2021). Kompozit yapılarda çatlak yayılımı: Sayısal analiz ve deneysel doğrulama. *Mühendislik Bilimleri Dergisi, 28*(4), 311–320.
4. Dzenis, Y. A., & Qian, J. (2001). Analysis of microdamage evolution histories in composites. *International Journal of Solids and Structures, 38*(10–13), 1831–1854. https://doi.org/10.1016/S0020-7683(00)00138-4
5. Gülsoy, M. (2019). *Fiber takviyeli kompozitlerde çekme davranışı ve çatlak ilerlemesi* [Master's thesis, İTÜ Fen Bilimleri Enstitüsü].
6. Hashin, Z., & Rotem, A. (1973). A fatigue failure criterion for fiber-reinforced materials. *Journal of Composite Materials, 7*(4), 448–464. https://doi.org/10.1177/002199837300700404
7. Hull, D., & Clyne, T. W. (1996). *An introduction to composite materials* (2nd ed.). Cambridge University Press.
8. Karahan, M., & Özdemir, U. (2020). Kompozit malzemelerde gerilme analizi ve deneysel inceleme. *Politeknik Dergisi, 23*(3), 841–850.
9. Kelly, A., & Zweben, C. (Eds.). (2018). *Comprehensive composite materials II*. Elsevier.
10. Kim, J. K., & Mai, Y. W. (1998). *Engineered interfaces in fiber reinforced composites*. Elsevier. https://doi.org/10.1016/B978-0-08-042695-2.X5000-3
11. Li, S. (2005). Modeling of adhesive interface cracking in composites. *Engineering Fracture Mechanics, 72*(7), 849–867.
12. Liu, D., & Nairn, J. A. (1990). Analytical and numerical modeling of fiber–matrix debonding in composites. *Mechanics of Materials, 9*(3), 123–133.
13. Muradov, R. A. (2021). Kompozit materiallarda çatların inkişafının riyazi modelleşdirilmesi. *AMEA-nın Xeberleri*, (3), 55–63.
14. Naumenko, K., & Altenbach, H. (2006). *Modeling of damage in composites*. Springer.
15. Panasyuk, V. V. (1987). *Mehanika razrusheniya kompozitsionnykh materialov* [Fracture mechanics of composite materials]. Naukova Dumka.
16. Reddy, J. N. (2003). *Mechanics of laminated composite plates and shells: Theory and analysis* (2nd ed.). CRC Press. https://doi.org/10.1201/b12409
17. Tay, T. E. (2008). Damage and failure of composite materials. *Composite Structures, 83*(1), 1–10.
18. Tsai, S. W., & Hahn, H. T. (1980). *Introduction to composite materials*. Technomic Publishing. https://doi.org/10.1201/9780203750148
19. Yıldız, M., & Karakuzu, R. (2007). Kompozit malzemelerde katmanlar arası delaminasyon analizi. *Makine Teknolojileri Elektronik Dergisi, 4*(1), 53–60.